Available online at www.sciencedirect.com
ScienceDirect
International Journal of Heat and Mass Transfer 51 (2008) 4637–4650
International Journal of HEAT and MASS TRANSFER
www.elsevier.com/locate/ijhmt

A mathematical model for analyzing the thermal characteristics of a flat micro heat pipe with a grooved wick

Kyu Hyung Do [a,c], Sung Jin Kim [a,*], Suresh V. Garimella [b]

[a] School of Mechanical, Aerospace, and Systems Engineering, KAIST, Daejeon 305-701, Republic of Korea
[b] School of Mechanical Engineering and Birck Nanotechnology Center, Purdue University, West Lafayette, IN 47907-2088, USA
[c] Energy Systems Division, Korea Institute of Machinery and Materials, Daejeon 305-343, Republic of Korea

Received 27 November 2007; received in revised form 21 February 2008
Available online 24 April 2008

Abstract

A mathematical model is developed for predicting the thermal performance of a flat micro heat pipe with a rectangular grooved wick structure. The effects of the liquid–vapor interfacial shear stress, the contact angle, and the amount of liquid charge are accounted for in the present model. In particular, the axial variations of the wall temperature and the evaporation and condensation rates are considered by solving the one-dimensional conduction equation for the wall and the augmented Young–Laplace equation, respectively. The results obtained from the proposed model are in close agreement with several existing experimental data in terms of the wall temperatures and the maximum heat transport rate. From the validated model, it is found that the assumptions employed in previous studies may lead to significant errors for predicting the thermal performance of the heat pipe. Finally, the maximum heat transport rate of a micro heat pipe with a grooved wick structure is optimized with respect to the width and the height of the groove by using the proposed model. The maximum heat transport rate for the optimum conditions is enhanced by approximately 20% compared to existing experimental results.

Keywords: Flat micro heat pipe; Grooved wick structure; Thin film evaporation; Thermal optimization

1. Introduction

Flat micro heat pipes have emerged as a reliable approach for cooling high-heat-flux electronic devices such as computer chips and thyristors. The International Technology Roadmap for Semiconductors 2005 [1] predicted that the allowable maximum power for high performance devices would exceed 300 W. Cao et al. [2] noted that heat fluxes generated by metal-oxide semiconductor-controlled thyristors are already in the range of 100 W/cm^2 to 300 W/cm^2. As the power density of critical electronic components increases, heat pipes with improved thermal performance are called for. In order to enhance the thermal performance of the heat pipe, it is necessary to identify and better understand the phenomena that govern its performance, and to optimize the wick structure of a micro heat pipe.

Many investigations have been conducted to characterize the thermal performance of micro/miniature heat pipes used for chip/module-level cooling of electronics. For predicting thermal characteristics of heat pipes with various cross-sectional and groove shapes, many researchers have suggested simplified one-dimensional theoretical models based on the differential form of the Laplace–Young equation [3–8]. In order to facilitate the analysis, these models employ many simplifying assumptions. First, evaporation and condensation are assumed to occur uniformly in the axial direction. Second, it is assumed that neither evaporation nor condensation occurs in the adiabatic section inside the heat pipe. Finally, the wall temperature is either assumed to be constant or its variation excluded from the analysis. These simplifying assumptions have good applicability to typical small heat pipes. Kim et al. [3] showed that

* Corresponding author. Tel.: +82 42 869 3043; fax: +82 42 869 8207.
E-mail address: sungjinkim@kaist.ac.kr (S.J. Kim).

0017-9310/$ - see front matter © 2008 Elsevier Ltd. All rights reserved.
doi:10.1016/j.ijheatmasstransfer.2008.02.039

Nomenclature

A	dispersion constant (J)
$\widehat{A}$	constant in Eq. (28)
a	coefficient defined in Eq. (21)
$\widehat{B}$	constant in Eq. (28)
b	coefficient defined in Eq. (21)
D	depth (m)
D_h	hydraulic diameter (m)
fRe	Poiseuille number
H	height (m)
h	heat transfer coefficient ($W\,m^{-2}\,K^{-1}$)
h_{fg}	latent heat of vaporization
K	curvature (m^{-1})
k	thermal conductivity ($W\,m^{-1}\,K^{-1}$)
L	length (m)
l	length of the extended meniscus region (m)
M	molecular weight ($kg\,mol^{-1}$)
$\dot{m}''$	mass flux ($kg\,s^{-1}\,m^{-2}$)
N	total number of grooves
P	perimeter (m)
p	pressure (Pa)
p_d	disjoining pressure (Pa)
Q	heat transport rate (W)
Q'	heat transfer rate per unit length ($W\,m^{-1}$)
q''	heat flux ($W\,m^{-2}$)
R	universal gas constant ($J\,mol^{-1}\,K^{-1}$)
r_c	capillary radius (m)
S	groove width (m)
s	coordinate parallel to the groove wall (m)
T	temperature (K) or fin thickness (m)
t	wall thickness (m)
u	velocity ($m\,s^{-1}$)
V	averaged interfacial velocity ($m\,s^{-1}$)
V_l	molar volume of the liquid ($m^3\,mol^{-1}$)
w	velocity ($m\,s^{-1}$)
x	coordinate along the heat pipe (m)

Greek symbols

α	groove wall inclination angle
δ	liquid film thickness (m)
Γ	mass flow rate ($kg\,s^{-1}$)
γ	solid–liquid contact angle
η	coordinate normal to the groove wall (m)
μ	dynamic viscosity (Pa s)
ν	kinematic viscosity ($m^2\,s^{-1}$)
ρ	density ($kg\,m^{-3}$)
σ	surface tension coefficient ($N\,m^{-1}$)
$\hat{\sigma}$	accommodation coefficient
τ	shear stress ($N\,m^{-2}$)

Subscripts

a	adiabatic section
amb	ambient
b	liquid block
c	condenser
cap	capillary
e	evaporator
f	fluid
i	interface
in	input
ini	initial
l	liquid
m	mean
max	maximum
men	meniscus region
min	minimum
r	remainder
s	solid
sat	saturation
t	total
thin	evaporating thin film region
v	vapor
w	wall

the temperature difference between the evaporator and condenser sections was less than 1 °C from their experimental results for 300 mm long heat pipes with outer diameters of 3 mm and 4 mm. However, as the size of a heat pipe decreases, the simplifying assumptions may lead to significant errors for predicting the thermal performance of the heat pipe. Hopkins et al. [4] experimentally showed that a 120 mm long flat heat pipe with an inner hydraulic diameter of 900 μm had a temperature drop from the evaporator to the condenser end cap of 25 °C at a heat load of 100 W. This suggests that the axial variations of the wall temperature and the evaporation and condensation rates should be taken into account to accurately predict the thermal performance of a micro heat pipe.

In the present study, a mathematical model is developed for accurately predicting the thermal performance of a flat micro heat pipe with a rectangular grooved wick structure. The effects of the liquid–vapor interfacial shear stress, the contact angle, and the amount of liquid charge are included in the proposed model. In particular, the axial variations of the wall temperature and the evaporation and condensation rates are considered by solving the one-dimensional conduction equation for the wall and the augmented Young–Laplace equation for the phase change process. In order to verify the model, the model predictions are compared to several existing experimental data. Using the results obtained from the proposed model, the validity of the simplifying assumptions employed in previous models is assessed. The effects of the amount of liquid charge and the axial wall conduction on the thermal performance of the heat pipe are also investigated. Finally, using the model developed, the maximum heat transport rate is

obtained and maximized to achieve optimal thermal performance from a flat micro heat pipe with a rectangular grooved wick structure.

2. Mathematical model

2.1. Governing equations

The system considered is a flat micro heat pipe with a rectangular grooved wick structure, as shown in Fig. 1. The governing equations are derived under the following assumptions: (i) one-dimensional steady incompressible flow along the length of the heat pipe; (ii) one-dimensional temperature variation in the wall of the heat pipe along the axial direction; and (iii) negligible convection in the liquid and vapor phases. In order to formulate the governing equations, the heat pipe is divided into a series of small control volumes (CV) of length dx. The continuity equations for the liquid and vapor regions are expressed as follows:

$$V_{\mathrm{v,i}}P_{\mathrm{v,i}} - A_{\mathrm{v}}\frac{\mathrm{d}u_{\mathrm{v}}}{\mathrm{d}x} = 0, \quad \text{in the vapor region} \tag{1}$$

$$-V_{\mathrm{l,i}}P_{\mathrm{l,i}} - A_{\mathrm{l}}\frac{\mathrm{d}u_{\mathrm{l}}}{\mathrm{d}x} = 0, \quad \text{in the liquid region} \tag{2}$$

$$\rho_{\mathrm{v}}V_{\mathrm{v,i}}P_{\mathrm{v,i}} = N\rho_{\mathrm{l}}V_{\mathrm{l,i}}P_{\mathrm{l,i}} \tag{3}$$

where $V_{\mathrm{v,i}}$, $P_{\mathrm{v,i}}$, A_{v}, and u_{v}, denote the averaged interfacial velocity (normal to the liquid–vapor interface), the perimeter at the liquid–vapor interface, the cross-sectional area, and the axial velocity for the vapor region in N grooves, respectively, while $V_{\mathrm{l,i}}$, $P_{\mathrm{l,i}}$, A_{l}, and u_{l}, denote the averaged interfacial velocity, the perimeter at the liquid–vapor interface, the cross-sectional area, and the axial velocity for the liquid flow in a groove, respectively.

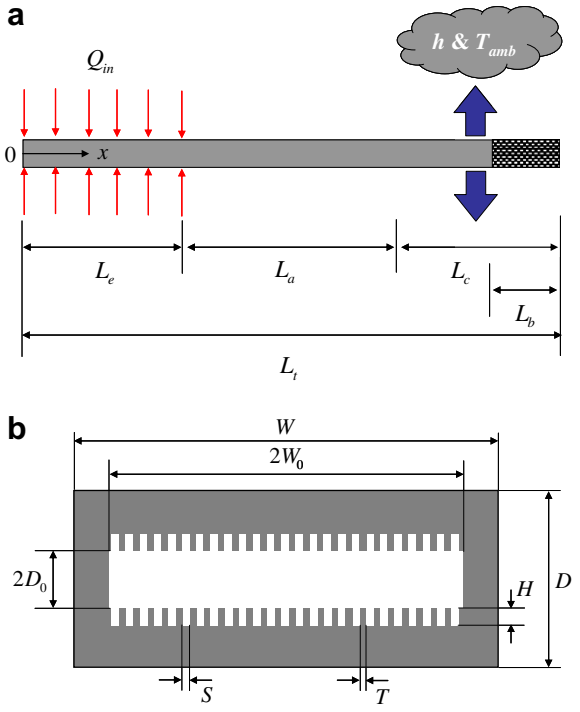

Fig. 1. Schematic diagrams of the flat heat pipe considered with a rectangular grooved wick structure: (a) overall dimensions, and (b) cross-sectional dimensions of the flat heat pipe.

From mass conservation across the interface, as shown in Eq. (3), the averaged interfacial velocity for the vapor phase can be expressed as

$$V_{\mathrm{v,i}} = \frac{N\rho_{\mathrm{l}}P_{\mathrm{l,i}}}{\rho_{\mathrm{v}}P_{\mathrm{v,i}}}V_{\mathrm{l,i}} \tag{4}$$

Most previous models determined the averaged interfacial velocity under the assumptions that evaporation and condensation occur uniformly in the axial direction and that neither evaporation nor condensation occurs in the adiabatic section [3–8]. Under these assumptions, the averaged interfacial velocity is expressed as

$$V_{\mathrm{v,i}} = \begin{cases} \frac{Q_{\mathrm{in}}}{\rho_{\mathrm{v}}h_{\mathrm{fg}}P_{\mathrm{v,i}}L_{\mathrm{e}}}, & 0 \leqslant x < L_{\mathrm{e}} \\ 0, & L_{\mathrm{e}} \leqslant x < L_{\mathrm{e}} + L_{\mathrm{a}} \\ -\frac{Q_{\mathrm{in}}}{\rho_{\mathrm{v}}h_{\mathrm{fg}}P_{\mathrm{v,i}}(L_{\mathrm{c}}-L_{\mathrm{b}})}, & L_{\mathrm{e}} + L_{\mathrm{a}} \leqslant x \leqslant L_{\mathrm{t}} - L_{\mathrm{b}} \end{cases} \tag{5}$$

However, Eq. (5) is no longer valid when the wall temperature varies along the axial direction or evaporation/condensation occur inside the heat pipe in the adiabatic section. Vadakkan et al. [9,10] demonstrated that there is no "adiabatic section" inside the heat pipe based on their numerical results. In the present model, the averaged interfacial velocity $V_{\mathrm{v,i}}$ is determined without invoking the specific assumptions used in previous studies, and is obtained by solving the augmented Young–Laplace equation and the mass flux model of Wayner et al. [11,12]. Details of the method for handling interfacial velocity are explained in the following section.

The conservation of axial momentum for incompressible vapor flow is written as

$$-2\rho_{\mathrm{v}}A_{\mathrm{v}}u_{\mathrm{v}}\frac{\mathrm{d}u_{\mathrm{v}}}{\mathrm{d}x} - (\tau_{\mathrm{v,w}}P_{\mathrm{v,w}} + \tau_{\mathrm{v,i}}P_{\mathrm{v,i}}) - A_{\mathrm{v}}\frac{\mathrm{d}p_{\mathrm{v}}}{\mathrm{d}x} = 0 \tag{6}$$

where $\tau_{\mathrm{v,w}}$ and $\tau_{\mathrm{v,i}}$ are the wall and interfacial shear stresses in the vapor region, respectively. Since the present model is one-dimensional, information about the wall and interfacial shear stresses is unknown. The velocity of the liquid phase is very small in comparison to that of the vapor phase, and so the interfacial shear stress for the vapor is computed by assuming the liquid to be stationary [7]. For a rectangular vapor duct, the values of the wall and interfacial shear stresses can be expressed using the following equation [13]:

$$\tau_{\mathrm{v,w}} = \tau_{\mathrm{v,i}} = \frac{24\mu_{\mathrm{v}}u_{\mathrm{v}}}{\pi^2 W_0}\frac{\sum_{n=1}^{\infty}\frac{(-1)^{n-1}}{(2n-1)^2}\tanh\left[\frac{(2n-1)\pi D_0}{2W_0}\right]}{\left[1-\frac{192}{\pi^5}\left(\frac{W_0}{D_0}\right)\sum_{n=1}^{\infty}\frac{1}{(2n-1)^5}\tanh\left[\frac{(2n-1)\pi D_0}{2W_0}\right]\right]} \tag{7}$$

The conservation of momentum for the liquid flow in a groove yields

$$\frac{dp_l}{dx} = -\frac{2\mu_l u_l}{D_{h,l}^2}(fRe)_l \tag{8}$$

For liquid flow, the inertial effects are negligible in comparison to those due to viscous losses [8]. The following correlation for $(fRe)_l$ for rectangular grooves was suggested by Schneider and DeVos [14]:

$$(fRe)_l = (fRe)_{l0}\left\{1 + \frac{D_{h,l}\tau_{v,i}}{\mu_l u_l} \times \frac{1}{3(2H/S)^2}[1 - 1.971\exp(-\pi H/S)]\right\} \tag{9}$$

where $(fRe)_{l0}$ corresponds to the case of no liquid–vapor interaction.

$$(fRe)_{l0} = \frac{8(2H/S)^2}{(1+2H/S)^2\left[\frac{1}{3} - \frac{64}{\pi^5(2H/S)}\tanh(\pi H/S)\right]}$$

In the present study, axial variation of the wall temperature is taken into account. In many previous models, the wall temperature is either assumed to be constant or not considered in the analysis [3–8]. This assumption may lead to significant errors for predicting the thermal performance of a heat pipe when the working fluid is overcharged, or when axial wall conduction is relatively large. The conservation of energy including the axial wall conduction is given as

$$k_s A_s \frac{d^2 T_w}{dx^2} - \rho_v V_{v,i} P_{v,i} h_{fg} + q''_w P_w = 0 \tag{10}$$

where k_s, A_s, T_w, P_w, h_{fg}, and q''_w are the thermal conductivity, the cross-sectional area, the temperature of the heat pipe wall, the outer wall perimeter of the heat pipe, the latent heat of vaporization, and the heat flux at the wall, respectively. The heat flux profiles at the wall can be expressed as follows:

$$q''_w(x) = \begin{cases} Q_{in}/P_w L_e, & 0 \leqslant x < L_e \\ 0, & L_e \leqslant x < L_e + L_a \\ -h[T_w(x) - T_{amb}], & L_e + L_a \leqslant x \leqslant L_t \end{cases} \tag{11}$$

where h denotes the heat transfer coefficient for convection between the external surface of the heat pipe and the ambient around the condenser section and is assumed to be constant. The heat transfer coefficient, h, is determined from the conditions that $\int_{L_e+L_a}^{L_t} h(T_w(x) - T_{amb})dx$ be equal to the input heat rate, Q_{in}.

In the liquid block region of Fig. 1(a), condensation does not occur because the vapor region and grooves are filled with liquid. Kim et al. [3] mentioned that the liquid block acts as a thermal barrier for condensation heat transfer due to its lower thermal conductivity. However, heat is still transferred by conduction from the liquid to the wall of the heat pipe. The present model accounts for heat transfer in this region. The heat transfer rate per unit length by conduction can be obtained by solving the two-dimensional conduction problem with geometry and boundary conditions shown in Fig. 2:

$$Q'_b = \frac{2N}{\pi}k_l(T_v - T_w(x))\sum_{n=1}^{\infty}\frac{1+(-1)^{n+1}}{n}\frac{-\cos(n\pi)}{\tanh(n\pi H/S)} \tag{12}$$

Therefore, the conservation of energy is applied over two regions, and Eq. (10) can be rewritten as

$$\begin{cases} k_s A_s \frac{d^2 T_w}{dx^2} - \rho_v V_{v,i} P_{v,i} h_{fg} + q''_w P_w = 0, & 0 \leqslant x \leqslant L_t - L_b \\ k_s A_s \frac{d^2 T_w}{dx^2} + Q'_b + q''_w P_w = 0, & L_t - L_b < x \leqslant L_t \end{cases} \tag{13}$$

The interfacial radius of the meniscus curvature is related to the pressure difference between the liquid and vapor by the Laplace–Young equation, which, in differential form, is

$$\frac{dp_v}{dx} - \frac{dp_l}{dx} = -\frac{\sigma}{r_c^2}\frac{dr_c}{dx} \tag{14}$$

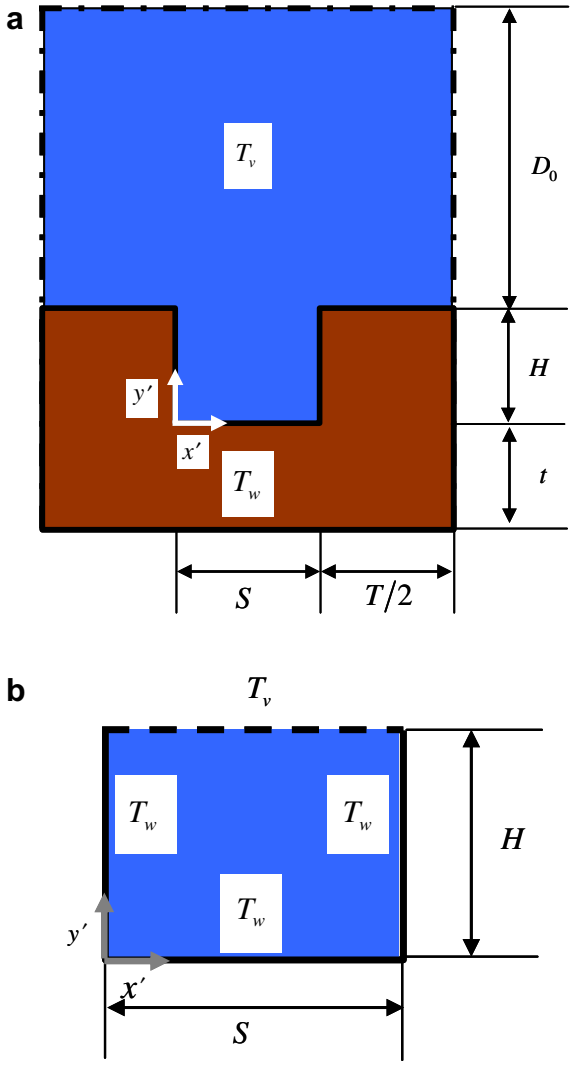

Fig. 2. Schematic cross-section of the liquid block region: (a) entire cross-section, and (b) computational domain.

Eqs. (1)–(3), (8), (13), (14) constitute a set of five first-order and one second-order nonlinear coupled ordinary differential equations in 7 unknowns: u_v, u_l, p_v, p_l, T_w, dT_w/dx, and r_c. The boundary conditions used at the beginning of the evaporator section are

$$r_c|_{x=0} = r_{c,\min} \tag{15}$$

$$u_l|_{x=0} = u_v|_{x=0} = 0 \tag{16}$$

$$p_v|_{x=0} = p_{sat}(T_v), p_l|_{x=0} = p_{sat}(T_v) - \sigma/r_{c,\min} \tag{17}$$

$$T_w|_{x=0} = T_{w,e}, \left.\frac{dT_w}{dx}\right|_{x=0} = 0 \tag{18}$$

Here p_v at $x = 0$ is taken to be the saturation pressure of the vapor at temperature T_v. If a heat pipe is to transport heat, a minimum capillary radius should be formed at the beginning of the evaporator section and a maximum capillary radius at the point where the liquid block starts in the condenser section [3]. It is assumed that the maximum capillary radius at $x = L_t - L_b$ equals the hydraulic radius of the vapor region [8], which is regarded as the convergence condition of the capillary radius. Eqs. (1)–(3), (8), (13), (14) are solved numerically, subject to the boundary conditions discussed.

2.2. Determination of the averaged interfacial velocity

As mentioned above, the assumptions that evaporation and condensation occur uniformly in the axial direction, that evaporation occurs only in the evaporator section, and that condensation occurs only in the condenser section are no longer valid when the wall temperature varies along the axial direction or when evaporation or condensation occurs inside the heat pipe in the adiabatic section. In this section, the method to determine the averaged interfacial velocity is explained.

2.2.1. Evaporation region

An evaporating film on a heat-loaded surface is considered, as shown in Fig. 3a. The extended meniscus formed on the heated wall may be characterized by three regions: (i) the adsorbed film region, where this film cannot evaporate due to the high adhesion forces; (ii) the evaporating thin film region (the so-called micro-region), where the major part of evaporation occurs; and (iii) the meniscus region, where the adhesion forces are negligible and the meniscus curvature radius is constant. In the evaporating thin film region, a one-dimensional laminar boundary layer approximation for the transverse liquid flow is used (see Fig. 3b). The mass flow rate is given as

$$\Gamma = \rho_l \int_0^{\delta} w_l \, d\eta = -\frac{\delta^3}{3\nu_l} \frac{dp_l}{ds} \tag{19}$$

where ν_l and δ are the kinematic viscosity and the liquid film thickness, respectively. Following Wayner et al. [11,12], the evaporative mass flux is modeled as a function of the temperature and pressure jumps at the interface according to the expression

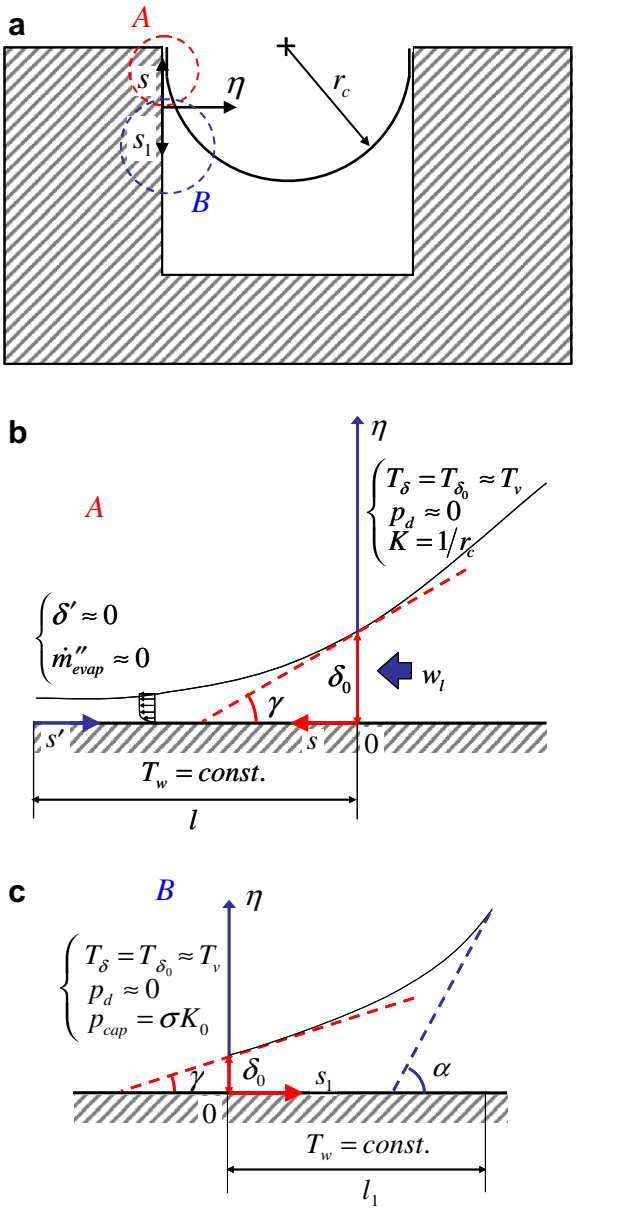

Fig. 3. Cross-section of the characteristic element of a heat pipe with a rectangular grooved wick structure (evaporation region): (a) cross-section of the liquid-filled groove, (b) evaporating thin film region, and (c) meniscus region.

$$\dot{m}''_{evap} = a(T_\delta - T_v) + b(p_l - p_v) \tag{20}$$

where T_δ is the temperature at the liquid–vapor interface, and T_v is the vapor temperature. The coefficients a and b are defined as

$$a = \frac{2\hat{\sigma}}{2-\hat{\sigma}} \left(\frac{M}{2\pi R T_\delta}\right)^{1/2} \left(\frac{p_v M h_{fg}}{R T_v T_\delta}\right),$$

$$b = \frac{2\hat{\sigma}}{2-\hat{\sigma}} \left(\frac{M}{2\pi R T_\delta}\right)^{1/2} \left(\frac{V_l p_v}{R T_\delta}\right) \tag{21}$$

where $\hat{\sigma}$ is the accommodation coefficient taken to be 1, M is the molecular weight, and V_l is the molar volume of the liquid. The liquid–vapor interfacial temperature and the

wall temperature are related by the one-dimensional conduction heat transfer equation as follows:

$$k_l \frac{T_w - T_\delta}{\delta} = \dot{m}''_{evap} h_{fg} \tag{22}$$

As Moosman and Homsy [15] suggested, Eqs. (20) and (22) may be combined to eliminate T_δ in favor of T_w:

$$\dot{m}''_{evap} = \left(1 + \frac{a h_{fg}}{k_l}\delta\right)^{-1} [a(T_w - T_v) + b(p_l - p_v)] \tag{23}$$

Substituting Eq. (23) into Eq. (22) yields

$$T_\delta = \left(a + \frac{k_l}{\delta h_{fg}}\right)^{-1} \left[k_l \frac{T_w}{\delta h_{fg}} + a T_v + b(p_v - p_l)\right] \tag{24}$$

The continuity equation for the evaporating liquid layer is

$$\frac{d\Gamma}{ds} = -\dot{m}''_{evap} \tag{25}$$

Substituting Eqs. (19) and (23) into Eq. (25) yields

$$-\frac{1}{3\nu_l}\frac{d}{ds}\left(\delta^3 \frac{dp_l}{ds}\right) = \left(1 + \frac{a h_{fg}}{k_l}\delta\right)^{-1} [a(T_w - T_v) + b(p_l - p_v)] \tag{26}$$

In the evaporating thin film region, the pressure difference between the vapor and liquid at the liquid–vapor interface is due to both the capillary and disjoining pressures, and is expressed by using the augmented Young–Laplace equation [12]:

$$p_v - p_l = p_d + \sigma \frac{d^2\delta}{ds^2}\left[1 + \left(\frac{d\delta}{ds}\right)^2\right]^{-3/2} \tag{27}$$

where the first term on the right-hand side is known as the disjoining pressure, and the second term is the capillary pressure, which is the product of the interfacial curvature, K, and the surface tension coefficient, σ.

Using the experimental data of Derjaguin and Zorin [16], Holm and Goplen [17] developed an expression for the disjoining pressure as a logarithmic function of the film thickness as follows:

$$p_d = -\rho_l R T_\delta \ln[\widehat{A}\delta^{\widehat{B}}] \tag{28}$$

For a water film on glass, the constants are given as $\widehat{A} = 1.49$ and $\widehat{B} = 0.0243$ [17]. However, for a water film on copper no data is available in the literature. As an alternative, we used the following approach. The disjoining pressure for non-polar liquids is expressed in terms of a polynomial function of the film thickness in the non-retarded form as [16]

$$p_d = A/\delta^3 \tag{29}$$

Even though this equation is commonly used for non-polar liquids, Wayner et al. [12] have applied it to a water film on glass with the dispersion constant A equal to 3.11×10^{-21} J. In the model developed here, Eq. (29) is used for determining the disjoining pressure, and the value of A for a water film on copper is calculated based on the Lifshitz theory [18] as $A = 5.043 \times 10^{-21}$ J.

In previous studies, Eqs. (26) and (27) for the evaporating thin film region were solved with boundary conditions being [19–22]

$$\delta|_{s'=0} = \delta_{ads}, \quad \delta'|_{s'=0} = 0, \quad (p_v - p_l)|_{s'=0} = p_d, \quad (p_v - p_l)'|_{s'=0} = 0 \tag{30}$$

However, the resulting solution is a trivial solution: $\delta = \delta_{ads} =$ constant. To obtain a non-trivial solution, previous investigators specified the boundary conditions at a point shifted away from the adsorbed film region. This leads to arbitrary changes in the boundary conditions and associated difficulties in the numerical treatment. In order to overcome these difficulties, Eqs. (26) and (27) are solved for the interval from the intersection of the evaporating thin film and the meniscus regions ($s = 0$) to the intersection of the evaporating thin film and the adsorbed film regions ($s = l$) with respective boundary conditions:

$$\delta|_{s=0} = \delta_0, \quad \delta'|_{s=0} = -\tan\gamma, \quad (p_v - p_l)|_{s=0} = \sigma K_0, \quad (p_v - p_l)'|_{s=0} = 0 \tag{31}$$

K_0 is the curvature in the meniscus region, and γ is the contact angle. The value of δ_0 is found from Eq. (29) when the disjoining pressure is negligibly small compared with the capillary pressure in the meniscus region: $p_d \approx 10^{-5}\sigma\ K_0$ at $\delta = \delta_0$. Although the initial-value problem, Eqs. (26) and (27) with BCs as in Eq. (31), is completely determined, its solution must satisfy an additional condition because the length of the evaporating thin film region is not specified:

$$\dot{m}''_{evap}|_{s=l} = 0 \tag{32}$$

Once δ and $(p_v - p_l)$ are determined, the evaporative mass flux and interfacial temperature profiles in the evaporating thin film region can be obtained, respectively, in Eqs. (23) and (24).

In the meniscus region shown in Fig. 3c, the liquid–vapor interfacial temperature is almost the same as the vapor temperature, and the disjoining pressure is negligible. The governing equation and boundary conditions are

$$\frac{d^2\delta}{ds_1^2} = K_0\left[1 + \left(\frac{d\delta}{ds_1}\right)^2\right]^{3/2} \tag{33}$$

$$\delta|_{s_1=0} = \delta_0, \quad \left.\frac{d\delta}{ds_1}\right|_{s_1=0} = \tan\gamma, \quad \left.\frac{d\delta}{ds_1}\right|_{s_1=l_1} = \tan\pi/2 \tag{34}$$

The evaporative mass flux in the meniscus region is

$$\dot{m}''_{evap} = \frac{k_l}{h_{fg}}\frac{T_w - T_v}{\delta} \tag{35}$$

Therefore, the averaged interfacial velocity in the evaporation region can be expressed as

$$V_{v,i} = \frac{2N}{\rho_v P_{v,i}}\left[\int_0^l \dot{m}''_{evap} ds + \int_0^{l_1} \dot{m}''_{evap} ds_1\right] \tag{36}$$

2.2.2. Condensation region

In the condensation region, the condensing film is divided into two regions, as shown in Fig. 4a: (i) a thin film region at the top of the fins and (ii) a meniscus region of constant curvature. To analyze heat transfer in the thin film region (see Fig. 4b), simplifying assumptions are employed. One assumption is that the film thickness variation along the s-axis is weak. The other assumption is that the disjoining pressure gradient along the liquid film can be neglected in comparison to that of the capillary pressure [21]. From these assumptions, the governing equation and boundary conditions for the film thickness at the top of the fins are given as

$$\frac{\sigma}{3\nu_l}\frac{\mathrm{d}}{\mathrm{d}s}\left(\delta^3\frac{\mathrm{d}^3\delta}{\mathrm{d}s^3}\right) = -\left(1+\frac{ah_{fg}}{k_l}\delta\right)^{-1}[a(T_w - T_v) + b(p_l - p_v)] \tag{37}$$

$$\left.\frac{\mathrm{d}\delta}{\mathrm{d}s}\right|_{s=0} = \left.\frac{\mathrm{d}^3\delta}{\mathrm{d}s^3}\right|_{s=0} = 0, \left.\frac{\mathrm{d}^2\delta}{\mathrm{d}s^2}\right|_{s=T/2} = \frac{1}{r_c}, \left.\frac{\mathrm{d}\delta}{\mathrm{d}s}\right|_{s=T/2} = -\tan\left(\frac{\pi}{2}-\gamma\right) \tag{38}$$

The boundary value problem, Eq. (37) with BCs as in Eq. (38), is solved approximately by introducing the following polynomial function for the film thickness [21].

$$\delta(s) = C_0 + C_1(s - T/2) + C_2(s - T/2)^2 + C_3(s - T/2)^3 + C_4(s - T/2)^4 \tag{39}$$

Using the boundary conditions in Eq. (38) the values of the coefficients can be determined as

$$C_1 = -\tan(\pi/2 - \gamma), \quad C_2 = 1/2r_c, \quad C_3 = 2C_4T, \quad C_4 = -\frac{C_1 - C_2T}{T^3} \tag{40}$$

From the condition that the total mass flow rate must be equal to that condensed in the region, $0 \leqslant s \leqslant T/2$, C_0 can be also obtained.

The difference between the vapor and liquid pressures, the condensation mass flux, and the interfacial temperature in the thin film region are respectively expressed as

$$p_v - p_l = \frac{A}{\delta^3} + \sigma\frac{\mathrm{d}^2\delta}{\mathrm{d}s^2} \tag{41}$$

$$\dot{m}''_{cond} = \left(1+\frac{ah_{fg}}{k_l}\delta\right)^{-1}[a(T_w - T_v) + b(p_l - p_v)] \tag{42}$$

$$T_\delta = T_w + \frac{\dot{m}''_{cond}h_{fg}\delta}{k_l} \tag{43}$$

In conjunction with Eq. (39), Eqs. (41)–(43) completely determine the problem.

The heat transfer problem for the meniscus region where condensation occurs, as shown in Fig. 4c, is very similar to that in the evaporation region, and its solution procedure will not be repeated here. The condensation mass flux in the meniscus region is written as

$$\dot{m}''_{cond} = \frac{k_l}{h_{fg}}\frac{T_w - T_v}{\delta} \tag{44}$$

Therefore, the averaged interfacial velocity in the condensation region can be expressed as

$$V_{v,i} = \frac{2N}{\rho_v P_{v,i}}\left[\int_0^{T/2}\dot{m}''_{cond}\mathrm{d}s + \int_0^{L_1}\dot{m}''_{cond}\mathrm{d}s_1\right] \tag{45}$$

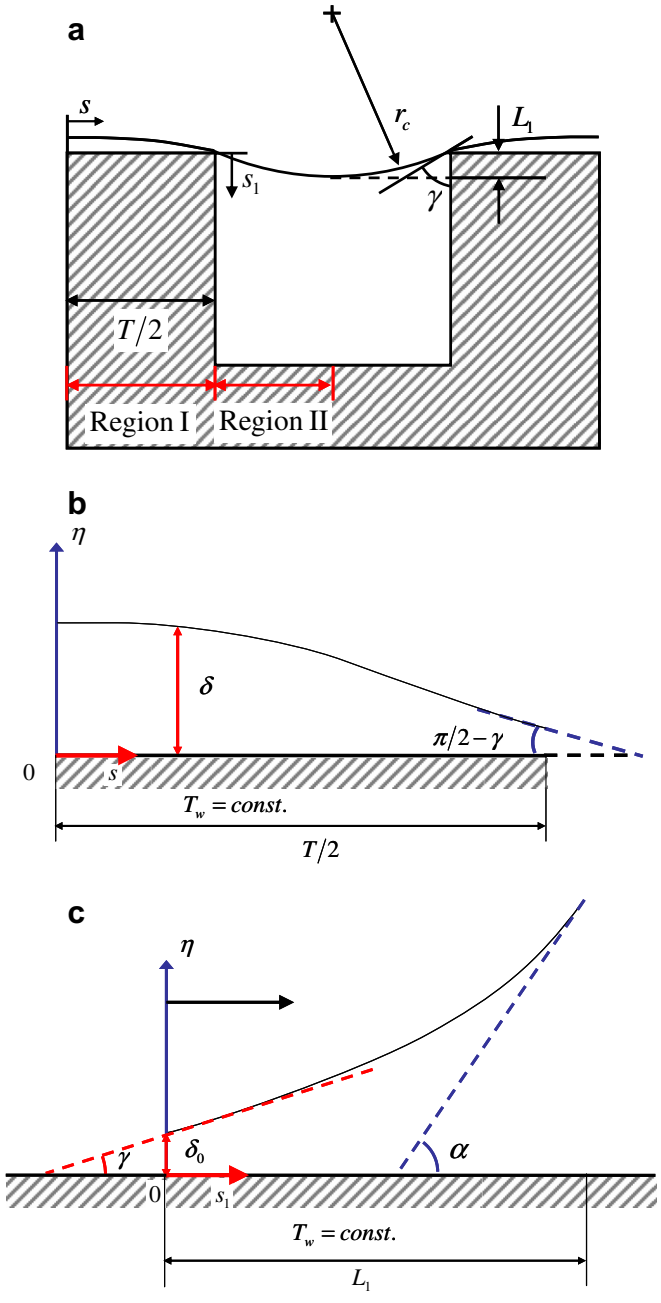

Fig. 4. Cross-section of the characteristic element of a heat pipe with a rectangular grooved wick structure (condensation region): (a) cross-section of the liquid-filled groove, (b) thin film region at the top of the fins, and (c) meniscus region.

2.2.3. Comparison of results from the model developed to those from Stephan and Busse [19]

To verify the model developed here for determining the heat transfer rates in the evaporating thin film and meniscus regions, a comparison is made with the numerical results of Stephan and Busse [19] for ammonia, using the following conditions: $T_v = 300$ K, $k_s = 221$ W/m^{2}K, $A = 2 \times 10^{-21}$ J, $H = 0.5$ mm, $T = 1$ mm, $t = 1$ mm, $r_c = 909.1$ μm, $\gamma = 19.7°$, $\alpha = 45°$, and $\Delta T = 1.31$ K. The results of the comparison are listed in Table 1. The heat transfer rates in the evaporating thin film and meniscus regions obtained from the present model are clearly seen to be in close agreement with Stephan and Busse's results.

2.3. Solution algorithm

When the flat heat pipe with a rectangular grooved wick structure is to transport the maximum amount of heat, a minimum capillary radius at the beginning of the evaporator section is defined by the following equation:

$$r_{c,\min} = \frac{S}{2\cos\gamma} \tag{46}$$

where γ denotes the minimum wetting contact angle, which is fixed for a specific working fluid/container combination [23]. The value of γ for a water/copper combination is 33° [24]. When the minimum capillary radius is given as Eq. (46), the complete solutions for the governing equations can be obtained by determining the maximum input heat load that satisfies the convergence condition. However, if the heat pipe is to transport a certain amount of heat which is smaller than its maximum heat capability, it is expected that the capillary radius at the beginning of the evaporator section is larger than that represented by Eq. (46). Therefore, when the input heat load is given, the complete solutions for Eqs. (1)–(3), (8), (13), (14) can be obtained by determining the minimum capillary radius that satisfies the convergence condition. The entire calculation procedure is summarized as follows:

When the heat pipe transports the maximum possible amount of heat:

(1) Determine $r_{c,\min}$ using Eq. (46).
(2) Assume an initial value of Q_{in} in Eq. (11) and the wall temperature at $x = 0$.
(3) Solve the governing equations, Eqs. (1)–(3), (8), (13), (14), using the fourth-order Runge–Kutta method.
(4) From 0 to x, calculate the total mass of the liquid in the grooves, m_l, and the vapor, m_v. Assume the remainder of the inner volume of the heat pipe is filled with liquid of mass m_r.
(5) If the overall mass balance condition, $m_l + m_v + m_r = m_{ini}$, is not satisfied, increase x to $x + \Delta x$ and return to step 3.
(6) If the overall mass balance condition is satisfied at a given value of x, calculate the liquid block length using $L_b = L_t - x$, and then solve the energy equation, Eq. (13), in the liquid block region. If the overall mass balance condition holds but the wall temperature gradient at $x = L_t$ is not zero, change the wall temperature at $x = 0$ (if $dT_w/dx|_{x=L_t} < 0$, increase the value of $T_w(0)$ and if $dT_w/dx|_{x=L_t} > 0$, decrease the value of $T_w(0)$) and return to step 3.
(7) If both the mass balance condition and the wall temperature gradient condition at $x = L_t$ are satisfied, check the convergence criterion. If the convergence criterion fails ($r_c(x = L_t - L_b) \neq r_{h,v}$), change Q_{in} (if $r_c(x = L_t - L_b) < r_{h,v}$, increase the value of Q_{in} and if $r_c(x = L_t - L_b) > r_{h,v}$, decrease the value of Q_{in}) and return to step 2.
(8) If the mass balance condition, the wall temperature gradient condition at $x = L_t$, and the convergence condition are all satisfied, regard Q_{in} as the maximum heat transport rate, Q_{max}, for the given minimum capillary radius and the specified working temperature.

When the heat pipe transports a specified amount of heat, $Q_{in} < Q_{max}$:

(1) Specify a value of Q_{in} in Eq. (11).
(2) Assume a minimum capillary radius, $r_{c,min}$ and the wall temperature at $x = 0$.
(3) Solve the governing equations, Eqs. (1)–(3), (8), (13), (14) using the fourth-order Runge–Kutta method.

Table 1
Comparison of the heat transfer rates obtained in the present study with those from [19]

	Stephan and Busse [19]	Present study
$\dot{q}_{in}$ (W/cm^2)	3.0	3.2
Q_{thin} (W/m)	13.5	14.1
Q_{men} (W/m)	16.5	18.0
Q_{thin}/Q_{men} (%)	45	43.9

Table 2
Specifications of the flat heat pipes with a rectangular grooved wick structure considered in the literature

	Hopkins et al. [4]	Lin et al. [5]
W (mm)	13.41	12.7
D (mm)	8.92	6.35
W_0 (mm)	4.875	5.13
D_0 (mm)	0.61	1.065
H (mm)	0.42	0.839
S (mm)	0.2	0.203
T (mm)	0.1	0.102
N (ea.)	62	64
L_e (mm)	15.6	18.5
L (mm)	70.0	50.6
L_c (mm)	34.4	32.5
Q_{in} (W)	0–120	0–150
T_v (°C)	60–95	90
Liquid fill (ml)	0.84	0.87

(4) From 0 to x, calculate the total mass of the liquid in the grooves, m_l, and the vapor, m_v. Assume the remainder of the inner volume of the heat pipe is filled with liquid of mass m_r.
(5) If the overall mass balance condition, $m_l + m_v + m_r = m_{ini}$, is not satisfied, increase x to $x + \Delta x$ and return to step 3.
(6) If the overall mass balance condition is satisfied at a given value of x, calculate the liquid block length using $L_b = L_t - x$, and then solve the energy equation, Eq. (13), in the liquid block region. If the overall mass balance condition holds but the wall temperature gradient at $x = L_t$ is not zero, change the wall temperature at $x = 0$ (if $dT_w/dx|_{x=L_t} < 0$, increase the value of $T_w(0)$ and if $dT_w/dx|_{x=L_t} > 0$, decrease the value of $T_w(0)$) and return to step 3.
(7) If both the mass balance condition and the wall temperature gradient condition at $x = L_t$ are satisfied, check the convergence criterion. If the convergence criterion fails ($r_c(x = L_t - L_b) \neq r_{h,v}$), change $r_{c,min}$ (if $r_c(x = L_t - L_b) < r_{h,v}$, increase the value of $r_{c,min}$. and if $r_c(x = L_t - L_b) > r_{h,v}$, decrease the value of $r_{c,min}$) and return to step 2.
(8) If the mass balance condition, the wall temperature gradient condition at $x = L_t$, and the convergence condition are all satisfied, regard $r_{c,min}$ as the mini-

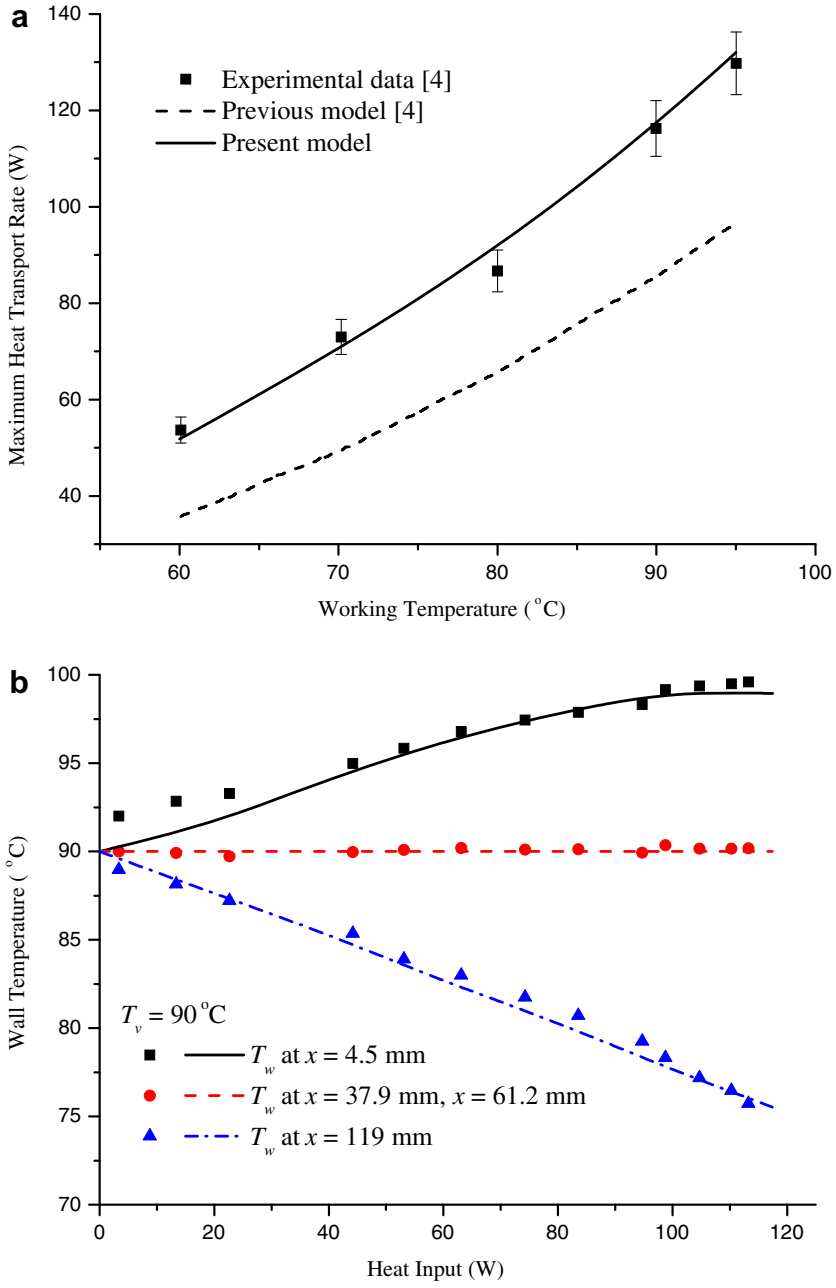

Fig. 5. Comparison of the model predictions with experimental data [4] ((symbols) experimental data and (lines) results from the present model): (a) maximum heat transport rate, and (b) wall temperature.

mum capillary radius, for the given input heat load, Q_{in}.

3. Results and discussion

3.1. Validation

In order to validate the model developed in the present work, the wall temperature profiles and the maximum heat transport rate obtained from the model are compared with experimental data of Hopkins et al. [4] and Lin et al. [5]. Geometric parameters of the experimental copper-water heat pipes and other relevant specifications of these experiments are summarized in Table 2. For numerical simulations, grid-independence tests are performed by changing dx. When the grid points are doubled from 300 (dx = 0.4 mm) in the axial direction, the maximum change in the velocity and temperature distributions is less than 1%. Therefore, dx is chosen to be 0.4 mm in the present study. Fig. 5a shows a comparison between the model predictions and experimental data of Hopkins et al. [4] for the maximum heat transport rate, and shows a maximum deviation of 5%. On the other hand, the maximum heat trans-

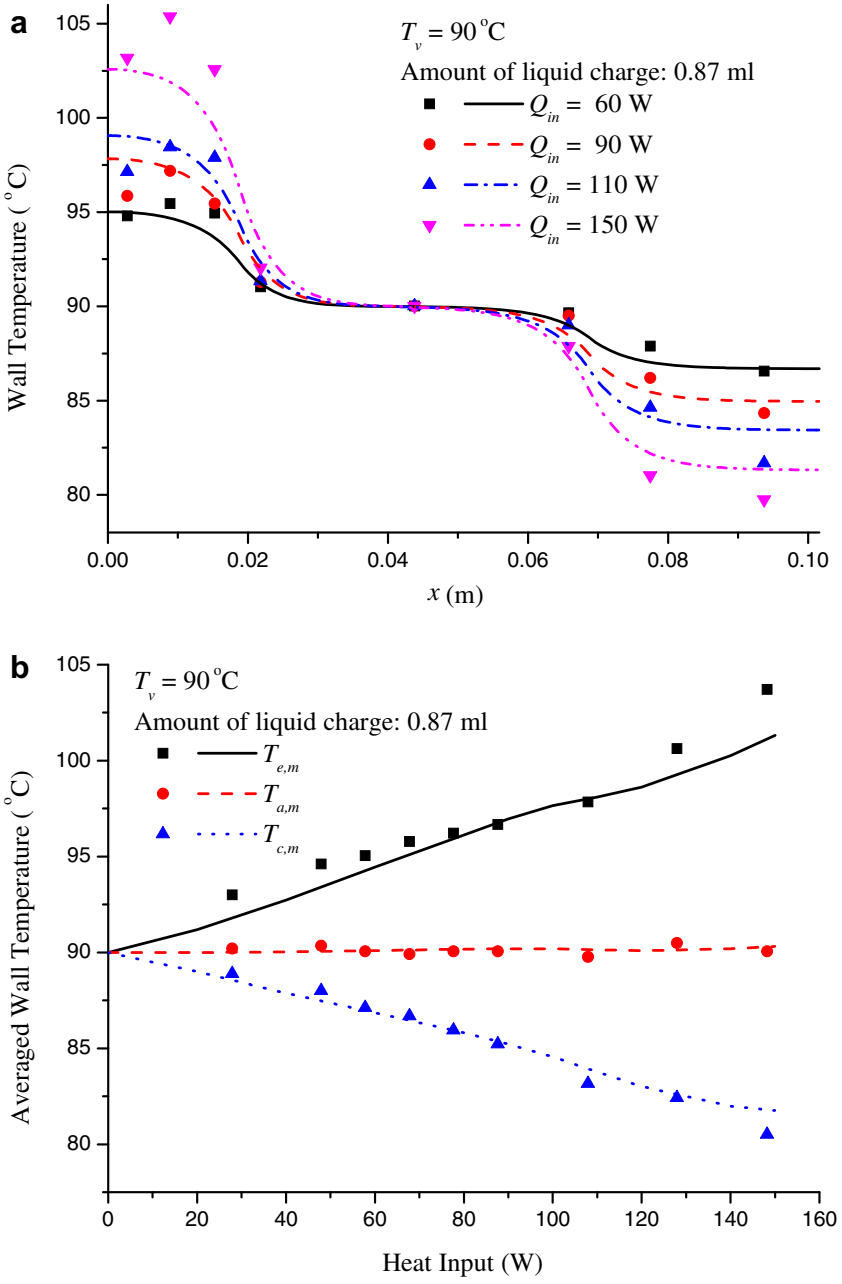

Fig. 6. Comparison of the model predictions with experimental data [5] ((symbols) experimental data and (lines) results from the present model): (a) wall temperature profiles, and (b) averaged wall temperature.

port rate obtained from the previous model [4] deviates substantially from the experimental results by over 30%. Fig. 5b shows a comparison of the model predictions with the experimental data for wall temperature. The discrepancy between the present model results and the experimental data is less than 2%.

A comparison of the model predictions and experimental data in [5] for the wall temperature profiles and the averaged wall temperatures is shown in Fig. 6. The agreement between the model and experimental results is again excellent. It is clear that the present model accurately predicts the wall temperature variation along the axial direction as well as the maximum heat transport rate obtained from previous experiments in the literature.

3.2. Discussion of the validity of commonly used simplifying assumptions

Fig. 7a illustrates the axial wall temperature profile for $Q_{in} = 100$ W and $T_v = 90$ °C. According to the results from the present model, the liquid block length in the flat heat pipe used in the experiments in [4] makes up approximately 58the condenser section. Substantial overcharging of the working fluid causes a large temperature drop in the liquid block region, as shown in Fig. 7a. This illustrates that the temperature drop in the liquid block region cannot be neglected when the working fluid is overcharged. Thus, the assumption of a constant wall temperature or the exclusion of wall temperature variation from the analysis, as

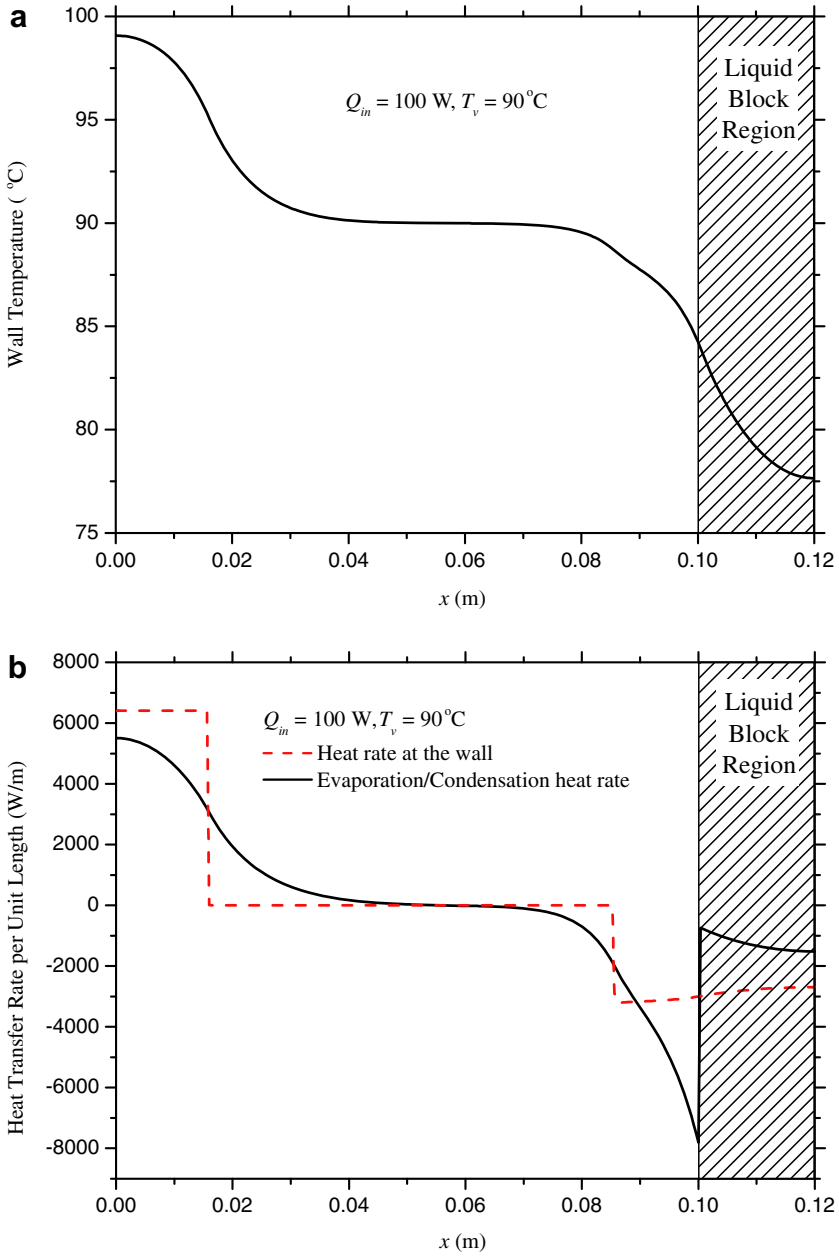

Fig. 7. Profiles ($Q_{in} = 100$ W, $T_v = 90$ °C): (a) wall temperature, and (b) heat transfer rate per unit length.

often adopted in past models, may lead to significant errors in predicting the wall temperature profiles. Profiles of the heat transfer rate per unit length along the axial direction are shown in Fig. 7b. As expected, evaporation and condensation rates are not uniform, but instead vary along the axial direction. Even in the so-called adiabatic section, heat transfer by evaporation or condensation takes place inside the heat pipe, as also pointed out in [9,10]. The influence of the solid thermal conductivity on the heat transfer rate per unit length profiles is evaluated in Fig. 8. The figure shows that as the solid thermal conductivity decreases, the evaporation (condensation) rate becomes more uniform along the axial direction and heat transfer by evaporation or condensation in the adiabatic section is negligible. Therefore, the assumption that neither evaporation nor condensation occurs in the adiabatic section is valid only if the effect of the axial wall conduction is negligible.

3.3. Effect of the amount of liquid charge

As mentioned above, the increase of the liquid block length results in a large temperature drop. To examine the effect of the amount of liquid charge on the thermal performance of the copper–water flat heat pipe the experimental configurations are chosen to be the same as those of Hopkins et al. [4]. The filling ratio is defined as the ratio of the liquid volume to the empty volume inside the heat pipe, and its original value used in their experiments is 0.4. When the filling ratio is 0.29, the liquid block length is zero. At the other extreme, the liquid block length is equal to the condenser section length for the filling ratio of 0.475. To evaluate the thermal performance of the heat pipe, the maximum heat transport rate and the thermal resistance are chosen as the objective functions. The thermal resistance, R, is defined here as the overall end cap to end cap temperature drop divided by the input heat load:

$$R = (T_{w,e} - T_{w,c})/Q_{in} \tag{47}$$

Fig. 9 illustrates the effect of the filling ratio on the maximum heat transport rate, Q_{max}, and the thermal resistance, R. As the filling ratio increases, Q_{max}, increases modestly. This is because flow friction decreases due to the decrease in the effective length of the heat pipe. The thermal resistance, on the other hand, shows a more significant increase with increasing filling ratio. When the filling ratio is 0.475 ($L_b = L_c$), Q_{max} is enhanced by approximately 19% compared with that for the filling ratio of 0.29 ($L_b = 0$). On the other hand, the thermal resistance is increased by approximately 160% over the same change in filling ratio. This means that the larger the filling ratio, the worse is the thermal performance of the heat pipe. Hence, the thermal performance of the heat pipe is maximized when the filling ratio is 0.29 ($L_b = 0$).

3.4. Thermal optimization of the heat pipe

In order to enhance the thermal performance of a heat pipe, an optimization of the grooved wick structure is performed to obtain the maximum heat transport rate. If the groove width S is reduced without changing the groove height H or the number of grooves, the fin thickness T will increase and the groove will take a narrower profile. This leads to a higher capillary pumping force. At the same time, however, the reduction of S causes a reduction of the cross-sectional area in the groove, which results in higher flow resistance. If H is increased without changing S or the number of grooves, the cross-sectional area in the vapor region will decrease. This leads to higher flow resistance in the

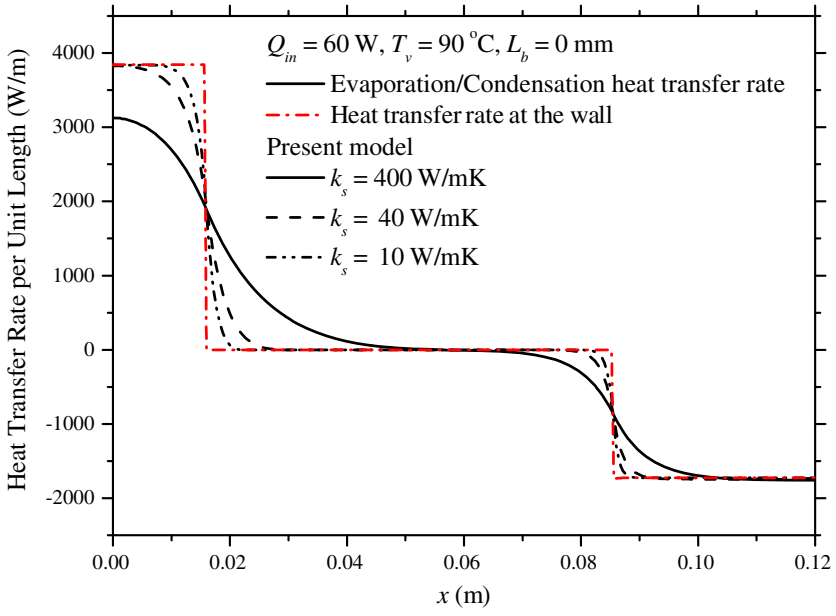

Fig. 8. Profiles of heat transfer rate per unit length profiles with respect to the solid thermal conductivity ($Q_{in} = 60$ W, $T_v = 90$ °C).

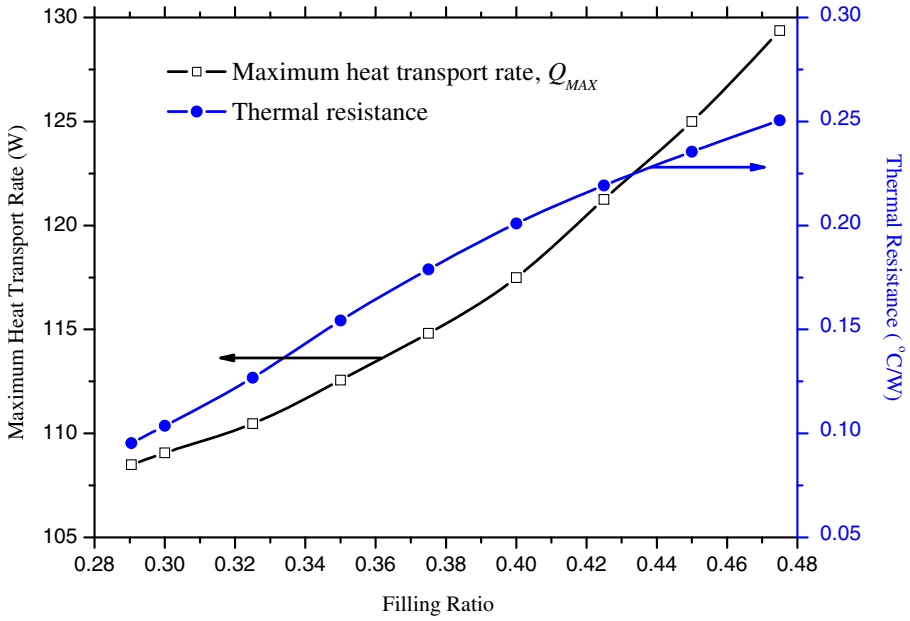

Fig. 9. Effect of the filling ratio on the maximum heat transport rate and the thermal resistance ($T_v = 90$ °C).

vapor region. On the other hand, the increase in H causes a reduction in the flow resistance in the groove because the additional flow resistance due to the liquid–vapor interfacial shear stress is decreased. These counteracting influences ultimately contribute to either an increase or a decrease in the thermal performance of the heat pipe. The effects of the optimization parameters S and H on the heat pipe performance are evaluated numerically by using the validated model and are shown in Fig. 10. It should be noted that experimental configurations of Hopkins et al. [4], such as the wall thickness of the heat pipe, the number of grooves, and the length of the heat pipe, are not changed in the optimization process. In addition, the initial liquid charge is chosen to have a value for which there is no excess liquid. This is because the thermal performance of the heat pipe is maximized when the liquid block length is zero, as mentioned in the previous section. From the results of the thermal optimization, a narrow, deep groove has higher heat

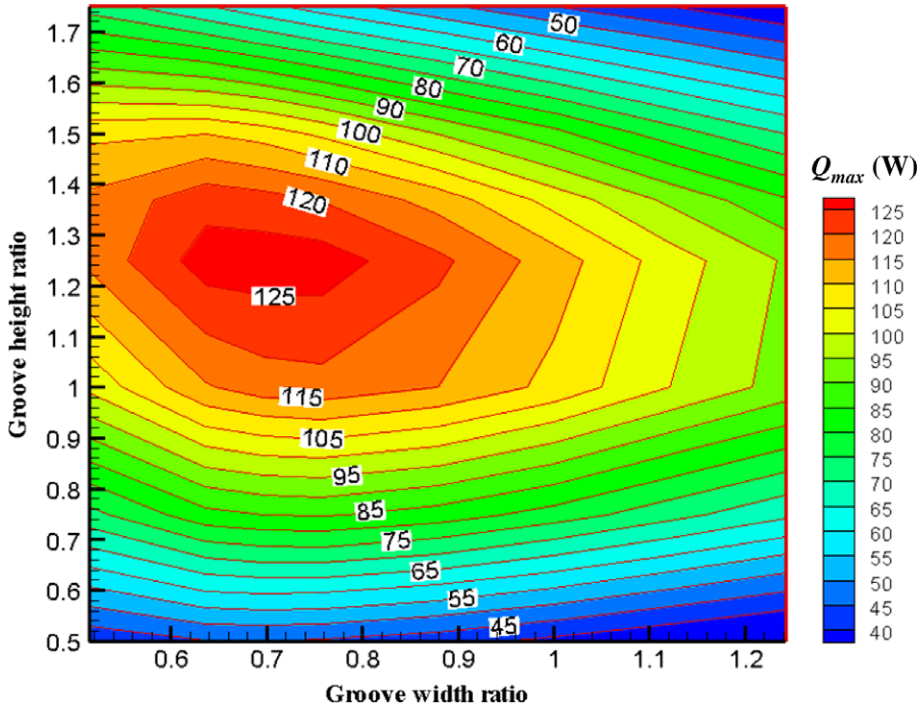

Fig. 10. Thermal optimization of the flat heat pipe for the maximum heat transport rate ($T_v = 90$ °C).

transport rate. For $T_v = 90$ °C, the maximum heat transport rate is 128 W with the optimum conditions of $S = 0.1437$ mm and $H = 0.525$ mm. The thermal performance of the optimized heat pipe can thus be enhanced by approximately 20% compared with the experimental results of Hopkins et al. [4].

4. Conclusions

A mathematical model is developed for accurately predicting the thermal performance of a flat micro heat pipe with a rectangular grooved wick structure. The effects of the liquid–vapor interfacial shear stress, the contact angle, and the amount of liquid charge have been included in the present model. In particular, the axial variations of the wall temperature and the evaporation and condensation rates have been considered by solving the one-dimensional conduction equation in the wall and the augmented Young–Laplace equation, respectively. The results obtained from the proposed model are in close agreement with published experimental results [4,5] for the wall temperature profiles and the maximum heat transport rate. From the validated model, it was found that the assumptions commonly employed in previous studies could lead to significant errors for predicting the thermal performance of the heat pipe. It is shown that the assumptions that evaporation and condensation occur uniformly in the axial direction, that evaporation occurs only in the evaporator section, and that condensation occurs only in the condenser section, are valid only if the axial wall conduction can be neglected. The effect of the amount of liquid charge on the thermal performance of the flat heat pipe has also been examined. As the amount of liquid charge increases, Q_{max} increases modestly due to a decrease in the effective heat pipe length, but the thermal resistance increases much more rapidly. Finally, the grooved wick structure is optimized using the proposed model for maximum heat transport rate with respect to the width and the height of the groove. The maximum heat transport rate is 128 W under the optimum conditions of $S = 0.1437$ mm and $H = 0.525$ mm for $T_v = 90$ °C, which reflects an enhancement of approximately 20% compared to the experimental result obtained by Hopkins et al. [4].

Acknowledgement

This work was supported by the Korea Science and Engineering Foundation (KOSEF) through the International Cooperation Program funded by the Ministry of Science and Technology (No. F01-2005-000-10072-0). Part of this work was conducted while the first and second authors were on a year-long research visit at Purdue University.

References

[1] International Technology Roadmap for Semiconductor (ITRS) 2005 [online] <http://www.itrs.net/>.
[2] Y. Cao, J.E. Beam, B. Donovan, Air-cooling system for metal oxide semiconductor controlled thyristors employing miniature heat pipes, J. Thermophys. Heat Transfer 10 (3) (1996) 484–489.
[3] S.J. Kim, J.K. Seo, K.H. Do, Analytical and experimental investigation on the operational characteristics and the thermal optimization of a miniature heat pipe with a grooved wick structure, Int. J. Heat Mass Transfer 42 (2003) 3405–3418.
[4] R. Hopkins, A. Faghri, D. Khrustalev, Flat miniature heat pipes with micro capillary grooves, ASME J. Heat Transfer 121 (1999) 102–109.
[5] L. Lin, R. Ponnappan, J. Leland, High performance miniature heat pipe, Int. J. Heat Mass Transfer 45 (2002) 3131–3142.
[6] B.R. Babin, G.P. Peterson, D. Wu, Steady-state modeling and testing of a micro heat pipe, ASME J. Heat Transfer 112 (1990) 595–601.
[7] J.P. Longtin, B. Badran, F.M. Gerner, A one-dimensional model of a micro heat pipe during steady-state operation, ASME J. Heat Transfer 116 (1994) 709–715.
[8] D. Khrustalev, A. Faghri, Thermal analysis of a micro heat pipe, ASME J. Heat Transfer 116 (1994) 189–198.
[9] U. Vadakkan, J.Y. Murthy, S.V. Garimella, Transient analysis of flat heat pipes, in: ASME Summer Heat Transfer Conference, July 21–23, Las Vegas, Nevada, 2003, HT2003-47349.
[10] U. Vadakkan, S.V. Garimella, J.Y. Murthy, Transport in flat heat pipes at high heat fluxes from multiple discrete sources, ASME J. Heat Transfer 126 (2004) 347–354.
[11] P.C. Wayner Jr., The effect of interfacial mass transport on flow in thin liquid films, Colloids Surf. 52 (1991) 71–84.
[12] P.C. Wayner Jr., K.Y. Kao, L.V. LaCroix, The interline heat transfer coefficient of an evaporating wetting film, Int. J. Heat Mass Transfer 19 (1976) 487–492.
[13] F.M. White, Viscous Fluid Flow, McGraw-Hill, 1991.
[14] G.E. Schneider, R. DeVos, Nondimensional analysis for the heat transport capability of axially-grooved heat pipes including liquid/vapor interaction, AIAA Paper, 1980, No. 80-0214.
[15] S. Moosman, G.M. Homsy, Evaporating menisci of wetting fluids, J. Colloid Interf. Sci. 73 (1) (1980) 212–223.
[16] B.V. Derjaguin, Z.M. Zorin, Optical study of the adsorption and surface condensation of vapours in the vicinity of saturation on smooth surface, in: J.H. Schlman (Ed.), Proceedings of the Second International Conference on Surface Activity, vol. 2, Butterwoods, London, 1957, pp. 145–152.
[17] F.W. Holm, S.P. Goplen, Heat transfer in the meniscus thin film transition region, ASME J. Heat Transfer 101 (1979) 543–547.
[18] J. Israelachvili, Intermolecular and Surface Forces, 2nd ed., Academic Press Inc., San Diego, CA, 1992.
[19] P.C. Stephan, C.A. Busse, Analysis of the heat transfer coefficient of grooved heat pipe evaporator walls, Int. J. Heat Mass Transfer 35 (2) (1992) 383–391.
[20] K.P. Hallinan, H.C. Chebaro, S.J. Kim, W.S. Chang, Evaporation from an extended meniscus for nonisothermal interfacial conditions, J. Thermophys. Heat Transfer 8 (4) (1994) 709–716.
[21] D. Khrustalev, A. Faghri, Heat transfer during evaporation on capillary-grooved structures of heat pipes, ASME J. Heat Transfer 117 (1995) 740–747.
[22] H. Wang, S.V. Garimella, J.Y. Murthy, Characteristics of an evaporating thin film in a microchannel, Int. J. Heat Mass Transfer 50 (2007) 3933–3942.
[23] A. Faghri, Heat Pipe Science and Technology, Taylor & Francis, Washington, 1995.
[24] V.G. Stepanov, L.D. Volyak, Y.V. Tarlakov, Wetting contact angles for some systems, J. Eng. Phys. 32 (1977) 1000–1003.